Journal of Alloys and Compounds 509 (2011) 8449–8454

Contents lists available at ScienceDirect

Journal of Alloys and Compounds

journal homepage: www.elsevier.com/locate/jallcom

Material flow and core/multi-shell structures in a friction stir welded aluminum alloy with embedded copper markers

W.F. Xu[a,b], J.H. Liu[b], D.L. Chen[a,*]

[a] Department of Mechanical and Industrial Engineering, Ryerson University, 350 Victoria Street, Toronto, Ontario M5B 2K3, Canada
[b] School of Materials and Engineering, Northwestern Polytechnical University, Xi'an 710072, PR China

ARTICLE INFO

Article history:
Received 19 March 2011
Received in revised form 28 May 2011
Accepted 31 May 2011
Available online 7 June 2011

Keywords:
Aluminum alloy
Friction stir welding
Material flow
Core–shell structure

ABSTRACT

The objective of this study was to reveal the material flow and temperature distribution in a thick aluminum plate during friction stir welding and examine the subsequent microstructural change with particular attention to the reaction between copper marker and aluminum matrix. It is shown that the material adjacent to the threaded pin was transported from the top to bottom non-symmetrically, and then was forced to move upwards at a small distance from the pin due to the constraint of an extrusion-die-like configuration. The interaction between the copper marker and aluminum matrix led to the formation of (i) a unique core/multi-shell microstructure consisting of copper core, inner shell of AlCu and outer shell of Al_2Cu, and (ii) a composite band containing uniformly-distributed Al_2Cu particles with refined grains due to the lower stacking fault energy of copper and the pinning role of Al_2Cu particles.

1. Introduction

Human-induced greenhouse gas emissions have recently been realized to be responsible for the increasing extreme precipitation events and devastating floods under global warming, which is known to be largely irreversible on timescales of many centuries [1,2]. Lightweighting in ground vehicles and aircraft is today one of the most important strategies to improve fuel economy and reduce anthropogenic environment-damaging emissions [3]. Aluminum alloy, being one of key lightweight structural materials with high strength-to-weight ratio, good machinability, environmental friendliness and recyclability, is desirable for structural components in the automotive and aerospace structures [4–7]. However, the structural applications of aluminum alloys inevitably involve welding and joining, which have been challenging using conventional fusion welding processes. The advent of a solid-state joining technique, called friction stir welding (FSW), invented by The Welding Institute of UK [8], provided an excellent opportunity for joining aluminum alloys. The technique has attracted considerable interest in the aerospace and other manufacturing industries since it is particularly suitable for welding lightweight metals (e.g., aluminum and magnesium alloys [9–12]). Using FSW the flaws (such as voids and hot cracks often occurred in the conventional fusion welding processes) can be avoided, thus effectively improving the integrity and longevity of welded joints.

During FSW the material undergoes intense plastic deformation at elevated temperatures, and the joint is created by frictional heating and the associated stirring or forging action of softened material as the tool moves along the joint interface. The tool geometry and welding parameters can significantly affect material flow pattern and temperature distribution [5,13], and subsequently govern the microstructure and properties of welded joints. Therefore, it is of vital importance to understand the plastic flow of materials during FSW. In the past few years several approaches, such as tracer technique using markers [14–16], welding of dissimilar materials [17–22], microstructural observations [5,14,23–25], have been used to visualize the complicated material flow pattern during FSW. Some computational methods including FEA [26–30] have been used to model the material flow as well. For example, Cui et al. [13] proposed a set of equations to describe the horizontal onion-ring-like plastic flow pattern and discussed the origin for the formation of such patterns in a longitudinal section. Seidel and Reynolds [15] embedded 1.8 mm thick AA5454-H32 marker material at both sides of faying surface (or weld centerline) at different locations of 8.1 mm thick AA2195-T8 alloy to reveal the flow pattern, and observed that the "stirring" of material occurred only at the top of the weld where the material transport was directly affected by the rotating tool shoulder. Schmidt et al. [16] studied the flow field of FSWed butt joints of 3 mm thick AA2024-T3 alloy using a CT imaging technique, where 0.1 mm thick copper marker material was inserted in the faying surface in-between the two work pieces to be welded and also in the direction perpendicular to the faying surface (viewed from the top of welds). Their observations provided the first experimental results support-

* Corresponding author. Tel.: +1 416 979 5000x6487; fax: +1 416 979 5265.
E-mail address: dchen@ryerson.ca (D.L. Chen).

0925-8388/$ – see front matter © 2011 Elsevier B.V. All rights reserved.
doi:10.1016/j.jallcom.2011.05.118

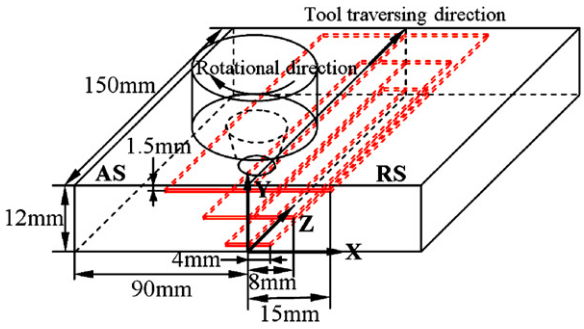

Fig. 1. Schematic illustration of the weld configuration with three parallel layers of copper strip markers (dashed lines) at different depths: top (Y = 10.5 mm), middle (Y = 6 mm), and bottom (Y = 2 mm).

ing the presence of the sticking condition at the interface between the threaded pin and softened material. A three-dimensional heat transfer and visco-plastic flow model was used to develop a criterion to identify the optimum tool shoulder diameter based on a principle of the maximum utilization of the applied torque for traction during FSW of AA6061 by Arora et al. [29]. However, the material flow during FSW has not been fully understood due to its complexity coupled with the presence of a non-uniform temperature distribution especially for a thick plate. It is unclear how high temperature could be achieved and what temperature gradient would be; what flow characteristics would be present in a thick plate and how the microstructure (grain size) would change when a copper marker is added into an aluminum alloy; and in particular whether the reaction between the marker material and the material to be welded would occur during FSW. The objective of this study was, therefore, to reveal the material flow and temperature distribution in a thick plate during FSW and examine the subsequent microstructural change with particular attention to the potential reaction between the marker and matrix material using multi-layer copper strips that were placed at different depths, as schematically indicated in Fig. 1.

2. Experimental

The weld was produced from two abutted plates of 12 mm thick AA2024-T4 aluminum alloy (rolled plate) with a chemical composition (in wt.%) of Al-3.9Cu-1.2Mg-0.3Mn-0.5Fe-0.5Si-0.25Zn-0.15Ti using a rotational rate of 300 rpm and a welding speed of 120 mm/min, with a welding tool title angle of 1.8°. The FSW tool had a shoulder of 26 mm in diameter and a threaded (left-handed screw) cone-shaped pin of 11.8 mm in root diameter and 8.3 mm in tip diameter.

Prior to welding 0.2 mm thick copper strips with different widths as marker material were inserted into the grooves at different positions, as shown in Fig. 1, where the grooves were made using electro-discharge wire cutting. Temperature changes in the weld region were measured using K-type thermocouples embedded at different positions through the drilled small holes with a diameter of 1.2 mm. A temperature transducer (SWP 8081) was used to amplify the milli-volt signals from the thermocouples into a range of 1–5 V (DC), and a computer was employed to collect and process the data [31].

JEOL 6380LV scanning electron microscope (SEM) coupled with Oxford energy dispersive X-ray spectrometry (EDS) operated in the back-scattered electron mode at 20 kV was used to examine the material flow and microstructure change of the welded joints. The phases formed during FSW were identified using X-ray micro-diffraction (PANalytical XRD with a mono-capillary of 0.3 mm in diameter in the incident beam path) using a Cu Kα radiation source at 45 kV and 40 mA. A ω-2θ scan was used to record the XRD patterns at room temperature, with a step size of 0.1° and time of 5 s in each step.

3. Results

3.1. Temperature profile

To understand the material flow behavior it is necessary to determine the temperature change experienced by the material near the welding tool. Fig. 2 shows the temperature profiles at different locations (Fig. 3(a)), where the coordinate origin is positioned at the intersection of weld centerline with the bottom surface (Fig. 1). The peak temperature at the advancing side (AS) (375 °C at point *a*, where the tool rotation was in the same direction as the translation of welding tool) was slightly higher than that at the retreating side (RS) (360 °C at point *e*, where the welding tool rotation and translational motion countered with each other). The peak temperatures at points *b*, *c* and *d* were about 463 °C, 422 °C and 392 °C, respectively, indicating that the peak temperature and temperature rise rate decreased from the top surface to the bottom surface of plate, accompanied by a temperature delay as well.

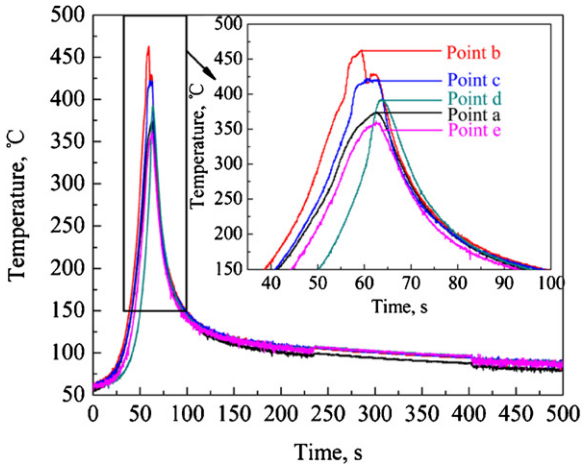

Fig. 2. Temperature versus time at different locations of the weld, (a) X = −13 mm, Y = 6 mm; (b) X = −6 mm, Y = 10.5 mm; (c) X = −6 mm, Y = 6 mm; (d) X = −6 mm, Y = 2 mm at the advancing side; (e) X = 13 mm, Y = 6 mm at the retreating side.

3.2. Material flow

Fig. 3 shows the backscattered electron images and EDS analysis from the cross-section of a FSWed specimen. It is seen from Fig. 3(a) that the intense deformation near the top surface caused break-up of the upper continuous copper strip into segments, and the remaining copper strip segments at both ends were extruded upwards by the surrounding material. This suggested the occurrence of upward material flow at a certain distance from the pin surface. Both at the intermediate thickness and near the bottom the copper strips were fragmented in the weld nugget zone (WNZ). In all cases small and large fragments were co-existent. The concave shape of the copper fragment movement in the WNZ (see Fig. 3(a)) indicated that the material adjacent to the pin surface flowed downwards. The material flow during FSW was mainly associated with the pin thread orientation and rotational direction [17,26,32].

3.3. Composite band and grain refinement

It is of interest to observe a band of composite-like structure formed adjoining the WNZ (mostly at the RS, as indicated by an arrow in Fig. 3(a)), which contained a large number of uniformly-distributed particles (Fig. 3(a) and (b)). EDS analysis revealed that they were Al_2Cu particles, to be further verified via XRD. Close examination indicated that the recrystallized grain size in the copper-rich composite band was smaller (~3 μm) than that in the rest of WNZ (~6 μm), as seen in Fig. 3(b). These phenomena will be discussed in Section 4.

3.4. Core/multi-shell structure

A special feature observed in the present study was the formation of a core/multi-shell microstructure occurred during FSW in

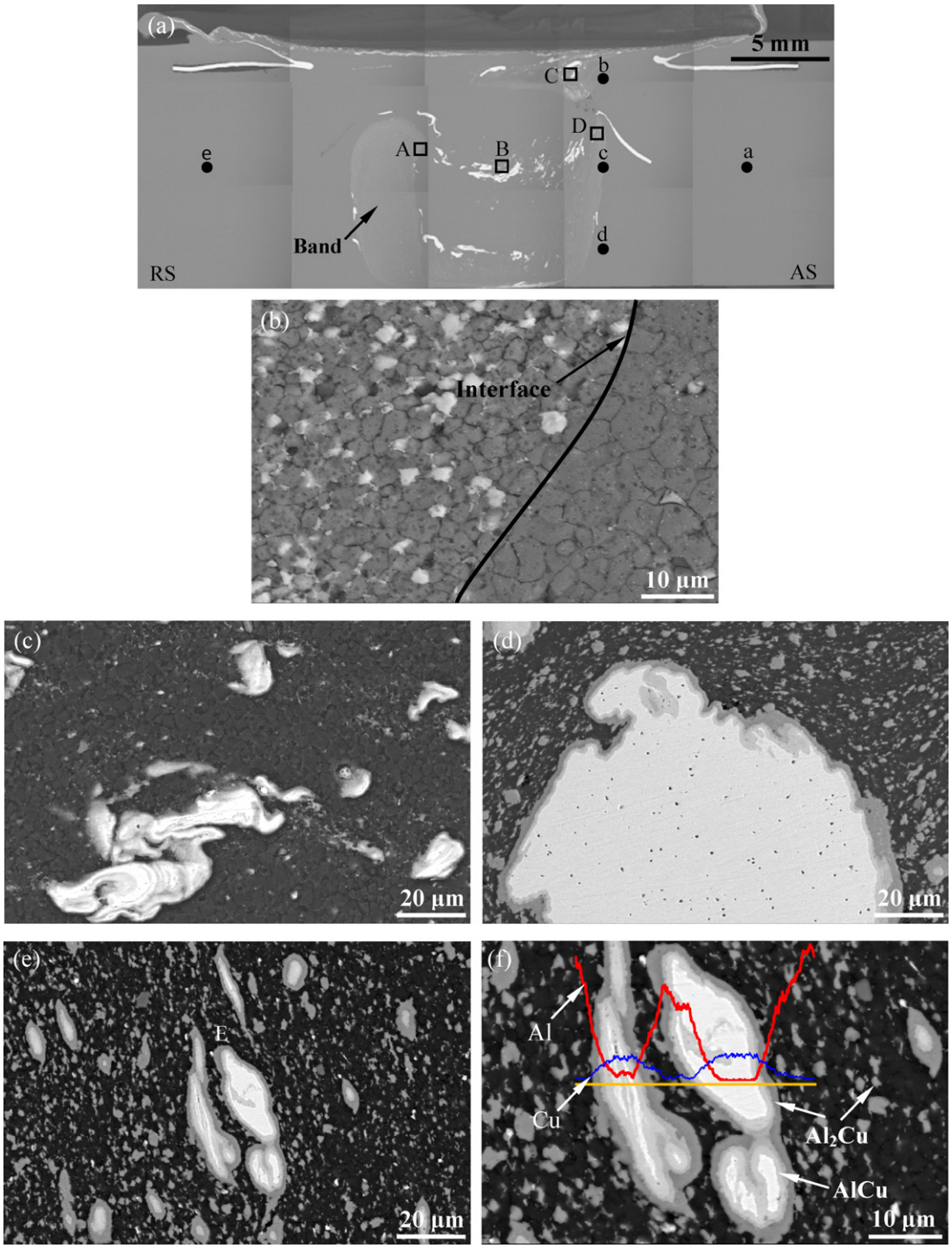

Fig. 3. Backscattered electron images of FSWed AA2024 joint, (a) overall view, where a, b, c, d and e indicate the thermocouple positions, (b) higher-magnification image of area A in (a), (c) higher-magnification image of area B in (a), (d) higher-magnification image of area C in (a), (e) higher-magnification image of area D in (a), and (f) EDS line scan across two large particles in area E in (e).

some larger copper fragment islands, as shown in Fig. 3(c)–(f) taken at different locations in the WNZ, where a white core and a shell with multiple gray levels were seen. It can be seen from Fig. 3(c) that the core/multi-shell structure in the weld center exhibited vortex-like deformation since the FSW could simply be thought to remove/scrape a layer of semi-cylinder in one revolution of the tool and the forward movement extruded the material from the advancing side to the retreating side of the tool [23]. EDS line scan in Fig. 3(f) revealed that the core was pure copper, whereas the shells contained a certain amount of copper. The inner shell adjacent to Cu core with an average width of ~2 μm was estimated via EDS point analysis to be AlCu phase since it contained ~52.1 at.% Cu and ~47.9 at.% Al, while the outer shell adjacent to the aluminum alloy matrix with an average width of ~2.5 μm was θ (Al_2Cu) phase as it had a composition of ~32.7 at.% Cu and 67.3 at.% Al, as shown in Fig. 4(a). These phases have been well established in the Al–Cu phase diagram [33]. The presence of both Al_2Cu and AlCu phases has also been observed in the WNZ when the dissimilar FSW of aluminum alloy to copper was conducted [34]. Similar core–shell structures have also been observed in Cu and Fe alloy powders

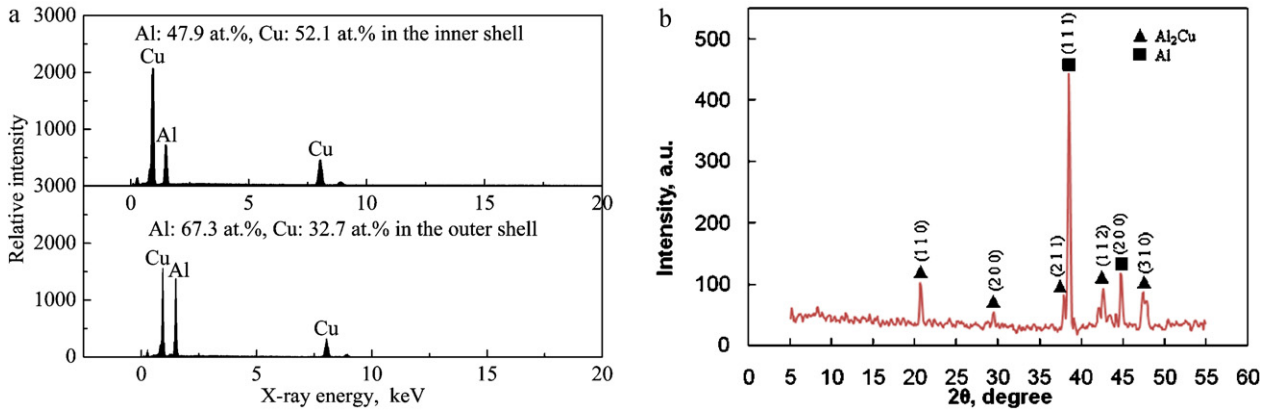

Fig. 4. (a) EDS analysis of the inner and outer shells corresponding to Fig. 3(f), and (b) X-ray micro-diffraction pattern of the composite band indicated by an arrow in Fig. 3(a).

via conventional gas atomization under gravity conditions [35]. To identify more accurately the phases, X-ray micro-diffraction (XRD) of the band structure was conducted, which further confirmed the occurrence of the Al_2Cu phase, as seen from five peaks shown in Fig. 4(b). It should be noted that the absence of AlCu peaks in the XRD pattern obtained using a ϕ0.3 mm micro-diffraction beam was due to its small amount present in the inner shell of the relatively large particles/fragments (Fig. 3(f)), which was believed to be below the detection limit of XRD [36–38]. On the other hand, there were many uniformly-distributed small particles which had become Al_2Cu phase as indicated by an arrow in Fig. 3(f). Therefore, the Al_2Cu peaks could be clearly seen from the XRD pattern, as shown in Fig. 4(b).

4. Discussion

The key issue of the temperature gradient occurred during FSW is first discussed. Compared with the RS, there was a slightly larger shear force at the AS, resulting in more friction heat. In addition, the smaller welding flash occurred at the AS led to less heat loss. As a result, the temperature was a little higher at the AS of the joint (Fig. 2). The higher temperature observed near the top surface was due to a combined action of both shoulder and threaded pin with the material. Since the shoulder had a higher linear velocity v ($v = \omega R$, ω is the rotational rate and R is the radius of the tool shoulder) than the pin with a smaller radius, additional friction heat was generated at the top surface. The transfer and dissipation of heat via thermal conduction from the top surface of the aluminum plate to the backing plate of the FSW machine was much faster than the heat loss by the heat convection between the top surface and atmosphere [31], which was also a time-dependent process. Therefore, the temperature gradient and delay occurred along the thickness of plate from the top to bottom surface, as shown in Fig. 2.

Next, the material flow along the thickness direction of a thicker plate is discussed. The higher temperature near the top surface (shown in Fig. 2) would make the material soften to a higher extent. In view of both the more softened material and the forward push force near point b in Fig. 3(a) stemming from the same rotational direction and welding direction, the transport of the material would be expected to start from the top surface at the AS. The softened material near the top surface was then dragged across the weld centerline and deposited in the composite band area at the RS. That is, the material in direct contact with the pin was driven downwards due to a combined action of the pin thread and clockwise rotation. During FSW the plasticized material adjoining the pin experienced two kinds of force. One was pressure F_P acting in the direction perpendicular to the thread surface due to the pin rotational thrust, and the other was traction force F_T which was parallel to the thread surface because of the presence of friction between the thread surface and the plasticized material, as schematically illustrated in Fig. 5. Under a combined action of those two forces (F_P and F_T) the plasticized material was driven to flow downwards from the top to the bottom along the direction of total force F (Fig. 5). Since the material flow during FSW was a constant volume process, and the shoulder, the pin, the backing plate and the undeformed base material created a case like extrusion die, then the material flow path had to be restricted. It follows that the material transported to the bottom area was forced to move upwards at a certain distance from the pin surface after filling out the potential cavity at the bottom. Similar observations were reported by Zhang et al. [24] as well. The formation of the composite bands in the border area of WNZ at both AS and RS was a result of the thorough stirring and forceful mixing of the plasticized material in the vicinity of threaded pin surface. The larger composite band present at the RS was a direct indication of the material flow from the top corner near the intersection between the pin and shoulder at the AS (i.e., near the location of b in Fig. 3(a) where the material exhibited a higher degree of softness caused by the highest temperature (Fig. 2), in conjunction with the stronger forward push or cutting force there) to the bottom spirally along a direction equivalent to F in Fig. 5.

The finer recrystallized grains observed in the copper-rich composite band (Fig. 3(a) and (b)) could be understood as follows. Copper had a lower stacking fault energy (SFE) in comparison with aluminum [39,40] (namely, ~41 mJ/m^2 for copper [41–43] versus 150–200 mJ/m^2 for aluminum [43–45]). The deformation mechanism was pointed out to go from slip via extended partial dislocations in the low SFE materials (or from perfect slip in the high

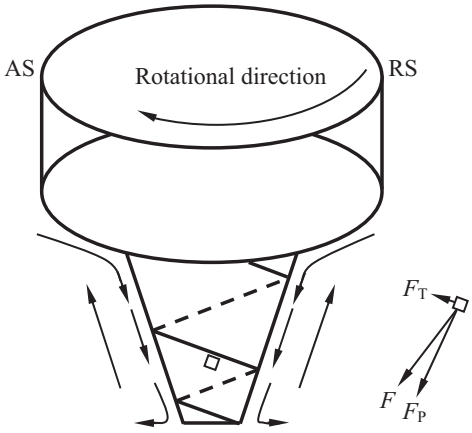

Fig. 5. Schematic illustration of the force analysis and flow of plasticized material adjacent to the threaded pin during FSW using a left-hand threaded pin tool rotating clockwise.

SFE materials) to grain-boundary-mediated processes as grain size decreased to the nanometer level [40]. Thus, the SFE has a significant influence on the deformation mechanism of materials. Balogh et al. [41] reported that the grain sizes decreased and the densities of dislocations and twins increased with decreasing SFE via increasing zinc content in copper–zinc alloys subjected to a severe plastic deformation process of high-pressure torsion. Likewise, the severely deformed grains during FSW were likely to retain their fine grain sizes due to the fact that the decrease in the SFE arising from the presence of copper in the aluminum alloy increased difficulties for cross-slip and resulted in a delay in the rate of recovery [41,44]. Indeed a relationship between the grain size, d, and SFE, γ_{SFE}, has been reported as [46]

$$\frac{d}{b} = A\left(\frac{\gamma_{SFE}}{Gb}\right)^{q}, \quad (1)$$

where b is the Burgers vector, G is the shear modulus, A and q are two dimensionless material constants. It is thus clear that grain refinement could be achieved by decreasing SFE. Similarly, Morishige et al. [44] demonstrated that the reduction in the SFE by magnesium solute atoms caused grain refinement in an aluminum–magnesium alloy via friction stir processing. It should be noted that, based on the above SFE considerations, the grain refinement tendency or capacity of copper in aluminum alloys used in the present study would be stronger than that of magnesium, since magnesium had about threefold higher SEF value of ~125 mJ/m^2 [47] than that of copper (~41 mJ/m^2) as mentioned earlier. Another important factor to refine the grain size in the composite band would be the pinning role (Zener pinning pressure) of the Al_2Cu particles which were mostly positioned at the grain boundaries, as seen from the left part of Fig. 3(b). This was due to the fact that the interaction between the particles and grain boundaries decreased grain boundary energy, thus reducing the driving force of grain boundary migration and restricting the grain growth. The pinning by dispersed particles was one of the well-recognized processes that reduced sufficiently the driving force for grain growth [48–53]. It has recently been confirmed via mesoscale grain growth models in conjunction with large-scale polycrystalline molecular dynamics simulations that even pinning only a fraction of boundaries was sufficient for the grain growth to be stopped since grain boundaries in polycrystalline materials formed an interconnected network [54]. As a result, very little grain growth could occur, leading to the finer recrystallized grains in the copper-rich composite band formed during FSW. Similar results were also reported in the literature [55,56], where Al_3Zr dispersed particles inhibited grain growth by pinning grain boundaries during hot deformation.

The formation of core/shell microstructure (Fig. 3(c) and (d)) was due to the interdiffusion between copper and aluminum atoms coupled with the intense plastic deformation. During FSW the material experienced the drastic deformation and thermal cycle with peak temperatures reaching 360–460 °C (Fig. 2). It was generally accepted that grain boundaries became the paths of more active electromigration or enhanced atomic diffusion for copper when the temperature reached above 300 °C [57], so that the diffusion of constituent atoms was inevitable. In general, diffusion coefficient D can be expressed as,

$$D = D_o \exp\left(-\frac{Q}{RT}\right), \quad (2)$$

where D_o is the frequency factor, Q is the activation energy for diffusion, R is the gas constant, and T is the absolute temperature. According to the Fick's law, diffusion distance L_D in the case of three-dimensional diffusion could be estimated as [58],

$$L_D = \sqrt{4Dt}, \quad (3)$$

where t is the diffusion time.

The peak temperature at point b (Figs. 2 and 3(a)) reached nearly 740 K, and the material in the WNZ (an immeasurable zone with thermocouples [31]) was estimated to experience temperatures about 773–828 K [28,59]. Based on Eqs. (2) and (3) the diffusion coefficient was estimated to be 2.8×10^{-13}–9.5×10^{-13} m^2/s and the diffusion distance L_D was approximately 3–6 μm using $D_o = 1.628 \times 10^{-5}$ m^2/s and $Q = 129.66$ kJ/mol [60]. This was in agreement with the width of shell observed (Fig. 3(f)). The small copper fragments were basically transformed into Al_2Cu particles (Fig. 4(b)) via the interdiffusion of Cu and Al atoms, which was further enhanced by the intense stirring or mixing during FSW. However, for the larger copper fragment islands (Fig. 3(f)) where L_D was smaller than their radius, the interdiffusion of constituent atoms could only occur at their surface to form multiple-layer shells consisting of inner AlCu and outer Al_2Cu phases. The minor volume phase was reported to form always the core part due to the Marangoni motion on the basis of the temperature dependence of the interfacial energy [35]. This was in agreement with the present findings where the minor phase of copper formed the core (Fig. 3(d)).

5. Conclusions

Three parallel copper strip markers were placed in the middle and near the top and bottom surfaces of the weld to reveal the material flow characteristics in the thickness direction of a thick plate of AA2024 aluminum alloy during FSW. The softened material adjacent to the threaded pin was transported from the top to the bottom non-symmetrically about the weld centerline under a combined action of pressure and traction force coming from the pin thread, and then was forced to move upwards at a small distance from the pin surface after filling the gap at the bottom due to the constraint of a closed extrusion-die-like configuration. The interaction of copper with aluminum matrix led to the formation of a composite band containing uniformly-distributed Al_2Cu particles in the border area of weld nugget zone. Compared to the advancing side, the composite band at the retreating side was larger as a result of the non-symmetrical material flow. The smaller grain size in the composite structure was attributed to the relatively low stacking fault energy of copper and the pinning role of Al_2Cu particles positioned mainly at grain boundaries. A unique core/shell microstructure consisting of irregularly-shaped and relatively-large copper islands and multiple-layer shells was observed to form due to the occurrence of interdiffusion during FSW, where the inner shell adjacent to the copper was AlCu and the outer shell next to the aluminum alloy was Al_2Cu.

Acknowledgements

This research was supported by Natural Sciences and Engineering Research Council of Canada (NSERC) and National Natural Science Foundation of China (NSFC grant No. 51075334) in the form of international research collaboration, and Foundation of Northwestern Polytechnical University for Graduate Visiting Abroad. D.L. Chen also acknowledges support from NSERC-DAS Award, Premier's Research Excellence Award, AUTO21 Network of Centers of Excellence, and Ryerson Research Chair program. The authors thank J.S. Yao, G.H. Luan, S.D. Bhole, Q. Li, A. Machin, J. Amankrah, R. Churaman for their assistance in the experiments and discussion.

References

[1] S.K. Min, X.B. Zhang, F.W. Zwiers, G.C. Hegerl, Nature 470 (2011) 378.
[2] P. Pall, T. Aina, D.A. Stone, P.A. Stott, T. Nozawa, A.G.J. Hilberts, Nature 470 (2011) 382.
[3] T.M. Pollock, Science 328 (2010) 986.

[4] P. Bala Srinivasan, K.S. Arora, W. Dietzel, S. Pandey, M.K. Schaper, J. Alloys Compd. 492 (2010) 631.
[5] R.S. Coelho, A. Kostka, F. dos Santos, A.R. Pyzalla, Adv. Eng. Mater. 12 (2008) 1127.
[6] P.S. De, R.S. Mishra, Metall. Meter. Trans. A 16 (2011) 343.
[7] K.T. Huang, T.S. Lui, L.H. Chen, J. Alloys Compd. 509 (2011) 7466.
[8] W.M. Thomas, E.D. Nicholas, J.C. Needham, M.G. Church, P. Templesmith, C.J. Dawes, GB Patent Application, No. 9,125,978.8, December 1991.
[9] B.L. Xiao, Q. Yang, J. Yang, W.G. Wang, G.M. Xie, Z.Y. Ma, J. Alloys Compd. 509 (2011) 2879.
[10] L.N. Yu, K. Nakata, J.S. Liao, J. Alloys Compd. 480 (2009) 340.
[11] H.W. Lee, T.S. Lui, L.H. Chen, J. Alloys Compd. 475 (2009) 139.
[12] F.Y. Hung, C.C. Shih, L.H. Chen, T.S. Lui, J. Alloys Compd. 428 (2007) 106.
[13] G.R. Cui, Z.Y. Ma, S.X. Li, Scripta Mater. 58 (2008) 1082.
[14] A.P. Reynolds, Sci. Technol. Weld. Joi. 5 (2000) 120.
[15] T.U. Seidel, A.P. Reynolds, Metall. Meter. Trans. A 32 (2001) 2879.
[16] H.N.B. Schmidt, T.L. Dickerson, J.H. Hattel, Acta Mater. 54 (2006) 1199.
[17] A.A.M. da Silva, E. Arruti, G. Janeiro, E. Aldanondo, P. Alvarez, A. Echeverria, Mater. Des. 32 (2011) 2021.
[18] A. Gerlich, P. Su, M. Yamamoto, T.H. North, Sci. Technol. Weld. Joi. 13 (2008) 254.
[19] R.M. Leal, C. Leitão, A. Loureiro, D.M. Rodrigues, P. Vilaca, Mater. Sci. Eng. A. 498 (2008) 384.
[20] C. Liu, D.L. Chen, S. Bhole, X. Cao, M. Jahazi, Mater. Charact. 60 (2009) 370.
[21] A. Abdollah-Zadeh, T. Saeid, B. Sazgari, J. Alloys Compd. 460 (2008) 535.
[22] T. Saeid, A. Abdollah-zadeh, B. Sazgari, J. Alloys Compd. 490 (2010) 652.
[23] K.N. Krishnan, Mater. Sci. Eng. A 327 (2002) 246.
[24] Z. Zhang, B.L. Xiao, D. Wang, Z.Y. Ma, Metall. Mater. Trans. A 42 (2011) 1717.
[25] L.M. Ke, C.P. Huang, L. Xing, K.H. Huang, J. Alloys Compd. 503 (2010) 494.
[26] A.P. Reynolds, Scripta Mater. 58 (2008) 338.
[27] A. Arora, Z. Zhang, A. De, T. DebRoy, Scripta Mater. 61 (2009) 863.
[28] R. Nandan, G.G. Roy, T. DebRoy, Metall. Mater. Trans. A 37 (2006) 1247.
[29] A. Arora, A. De, T. DebRoy, Scripta Metall. 64 (2011) 9.
[30] P.F. Mendeza, K.E. Tello, T.J. Lienert, Acta Mater. 58 (2010) 6012.
[31] W.F. Xu, J.H. Liu, G.H. Luan, C.L. Dong, Mater. Des. 30 (2009) 1886.
[32] S.M. Chowdhury, D.L. Chen, S.D. Bhole, X. Cao, Mater. Sci. Eng. A 527 (2010) 6064.
[33] M. Aravind, P. Yu, M.Y. Yau, D.H.L. Ng, Mater. Sci. Eng. A 380 (2004) 384.
[34] H.J. Liu, J.J. Shen, L. Zhou, Y.Q. Zhao, C. Liu, L.Y. Kuang, Sci. Technol. Weld. Joi. 16 (2011) 92.
[35] C.P. Wang, X.J. Liu, I. Ohnuma, R. Kainuma, K. Ishida, Science 9 (2002) 990.
[36] T.S. Kim, H.S. Kim, T.G. Kim, H.G. Jeong, S.J. Hong, J. Alloys Compd. 483 (2009) 593.
[37] P. Nel, D. Lau, D. Hay, N. Wright, Nucl. Instrum. Methods Phys. Res. B 251 (2006) 489.
[38] D.L. Bish, S.J. Chipera, Clays Clay Miner. 39 (1991) 437.
[39] S. Ogata, J. Li, S. Yip, Science 298 (2002) 807.
[40] H. Van Swygenhoven, P.M. Derlet, A.G. Frseth, Nat. Mater. 3 (2004) 399.
[41] L. Balogh, T. Ungár, Y.H. Zhao, Y.T. Zhu, Z. Horita, C. Xu, T.G. Langdon, Acta Mater. 56 (2008) 809.
[42] C.B. Carter, I.L.F. Ray, Philos. Mag. 35 (1977) 189.
[43] M.F. de Campos, Mater. Sci. Forum 591 (2008) 708.
[44] T. Morishige, T. Hirata, T. Uesugi, Y. Takigawa, M. Tsujikawa, K. Higashi, Scripta Mater. 64 (2011) 355.
[45] G.E. Dieter, Mechanical Metallurgy, third ed., McGraw-Hill, Boston, 1986.
[46] F.A. Mohamed, Acta Mater. 51 (2003) 4107.
[47] R.N.V. Kumar, J.J. Blandin, C. Desrayaud, F. Montheillet, M. Suery, Mat. Sci. Eng. A 359 (2003) 150.
[48] A.R. Eivani, S. Valipour, H. Ahmed, J. Zhou, J. Duszczyk, Metall. Mater. Trans. A 42A (2011) 1109.
[49] R.D. Doherty, D.J. Srolovitz, A.D. Rollett, M.P. Anderson, Scripta Metall. 21 (1987) 675.
[50] M. Miodownik, E.A. Holm, G.N. Hassold, Scripta Mater. 42 (2000) 1173.
[51] M. Apel, B. Böttger, J. Rudnizki, P. Schaffnit, I. Steinbach, ISIJ Int. 49 (2009) 1024.
[52] F.J. Humphreys, M.G. Ardakani, Acta Mater. 44 (1996) 2717.
[53] T. Nishizawa, I. Ohnuma, K. Ishida, Mater. Trans. 38 (1997) 950.
[54] E.A. Holm, S.M. Foiles, Science 328 (2010) 1138.
[55] M. Cabibbo, E. Evangelista, S. Spigarelli, Metall. Mater. Trans. A 35 (2004) 293.
[56] K.T. Kashyap, Bull. Mater. Sci. 24 (2001) 643.
[57] K.C. Chen, W.W. Wu, C.N. Liao, L.J. Chen, K.N. Tu, Science 321 (2008) 1066.
[58] J. Weertman, J. Glaciol. 7 (1968) 161.
[59] Y.S. Sato, M. Urata, H. Kokawa, Metall. Mater. Trans. A 33 (2002) 625.
[60] T.C. Wei, A.R. Daud, Microelectron. Int. 19 (2002) 38.